Modeling Atomic Layer Deposition of Alumina Using Reactive Force Field Molecular Dynamics

Devon Romine[1], Ridwan Sakidja[1]

[1] Missouri State University

Abstract

In this study, we have utilized the reactive molecular dynamics (MD) simulations to model the Atomic Layer Deposition (ALD) process that forms an ultra-thin film of a tunnel barrier made of amorphous alumina. We chose the reactive MD approach over the ab-initio molecular dynamics simulation used in previous studies due to its lower computational cost, its ability to model over a relatively longer simulation period and its capability to assess atomistic-based dynamics for a larger substrate. We have reviewed the capabilities of ReaxFF to model stable precursors and reactions paths for two surface reactions of the ALD process utilizing LAMMPS and Amsterdam Modeling Suites (AMS) software. A comparison of two force field potential models is also made in an effort to determine where deficiencies in the modeling capabilities lie.

The support of NSF (Grant No. 1809284) from the Electronics, Photonics and Magnetic Devices (EPMD) Program is gratefully acknowledged. We also thanks to NERSC for the computational support.

Introduction

Atomic layer deposition (ALD) is a thin-film deposition technique in which sequential interactions between precursors and the surface build a substrate one atomic layer at a time. The self-terminating nature of the precursor/surface reaction allows for oversaturation of the surface area while still building a uniform thin film. The control over the layer thickness that ALD provides has become essential in the development of microelectronics like tunnel barrier junctions. [1, 2]

The atomic layer deposition of aluminum oxide using gas phase Trimethylaluminum (TMA $Al(CH_3)_3$) and H_2O is a vital role in the development of effective tunnel barriers due to alumina's high band gap of approximately 9**eV** [3]. Many studies of the mechanisms have been done using experimental techniques [4-8] and computational DFT calculations [3, 9-11]. The largest shortcoming of QM calculations like DFT and Ab Initio, is that they are computationally rigorous and can only simulate small scale models (couple hundred atoms). Reactive Force Field (ReaxFF) MD simulations are a classical approach to QM modeling and can accurately simulate large scale models (a couple thousand atoms) over larger time scales. This opens pathways to computational studies of aggregate mechanics of precursors and the effects oversaturation has on the ALD process at the atomistic scale.

The overall reaction $2\mathrm{Al(CH3)3} + 3H_2O \rightarrow Al_2O_3 + 3CH_4$ can be broken into two half-reactions

A) $Al - OH^S + Al(CH_3)_3 \rightarrow Al - O - Al(CH_3)_2{}^S + CH_4$

B) $Al - CH_3^S + H_2O \rightarrow Al - OH^S + CH_4$

Where S denotes the surface species. The first half reaction is TMA interacting with the hydroxylated surface through the mechanism of ligand exchanges between TMA and the Hydrogen of the surface hydroxyl units. The methyl units then form methane (CH_4) with the Hydrogen and the remaining Al and methyl units dissociate. The TMA/Alumina pulse is self-terminating due to the steric nature of the methyl groups and will deposit until there is no more open area for the methyl groups. The second half reactions are gas phase water interacting with methyl aluminum surface. They form ligand exchanges with all the remaining methyl groups on the surface forming methane gas, then dissociate onto the oxygen bridges, forming a bilayer of alumina and aluminum hydroxide. [1, 2] The deposition of alumina for tunnel junction barriers occurs in the effective temperature range of 150-200 °C [5-8], some successful depositions have occurred at temperatures as low as 33 °C and can be optimal up to 350 °C [4, 12].

Presented here is a comparison of the ability of two currently available Reactive Force Field (ReaxFF) potentials to assess their capabilities to model the ALD process. A review of the precursor stability and ALD reaction pathways was conducted using the ReaxFF MD simulations to determine the deficiencies and strengths of using ReaxFF as a modeling method. **Studies involving other methods of modeling the deposition of alumina have been conducted and notable advantages in the ReaxFF potentials are present. Advantages including accurate charge separation at the metal-oxide interface and the ability to reproduce self-limiting nature of the deposition, an important part of the ALD process that is observed experimentally.[13]**

Computational Methods

The ReaxFF MD simulations were calculated using the LAMMPS code [14]. A timestep of 0.25 fs was used in all MD simulations and the OVITO [15] software was used to visualize them. The ReaxFF Geometry Optimizations were carried out at 0K, using the BFGS Quasi-Newtonian optimization method available in the Amsterdam Modeling Suites (AMS) [16, 17]. To determine the importance of transferability in ReaxFF potentials, two models are used. Model 1 uses force field potentials developed by Hong et al. [18] for modeling carbon coating on Al nanoparticles using hydrocarbons, and model 2 uses force field potentials developed by Zheng et al. [19] developed to model ALD on Ge using TMA and H_2O as precursors. **Vienna ab initio simulation package (VASP)[20] DFT calculations were performed to confirm the accuracy of the optimizations. The PBE[21] functional in the projector augmented-wave (PAW)[22] method with an energy cutoff of 520 eV, gaussian smearing (σ=0.05), and a 1x1x1 k-point grid were used in optimizing the geometry of the systems.**

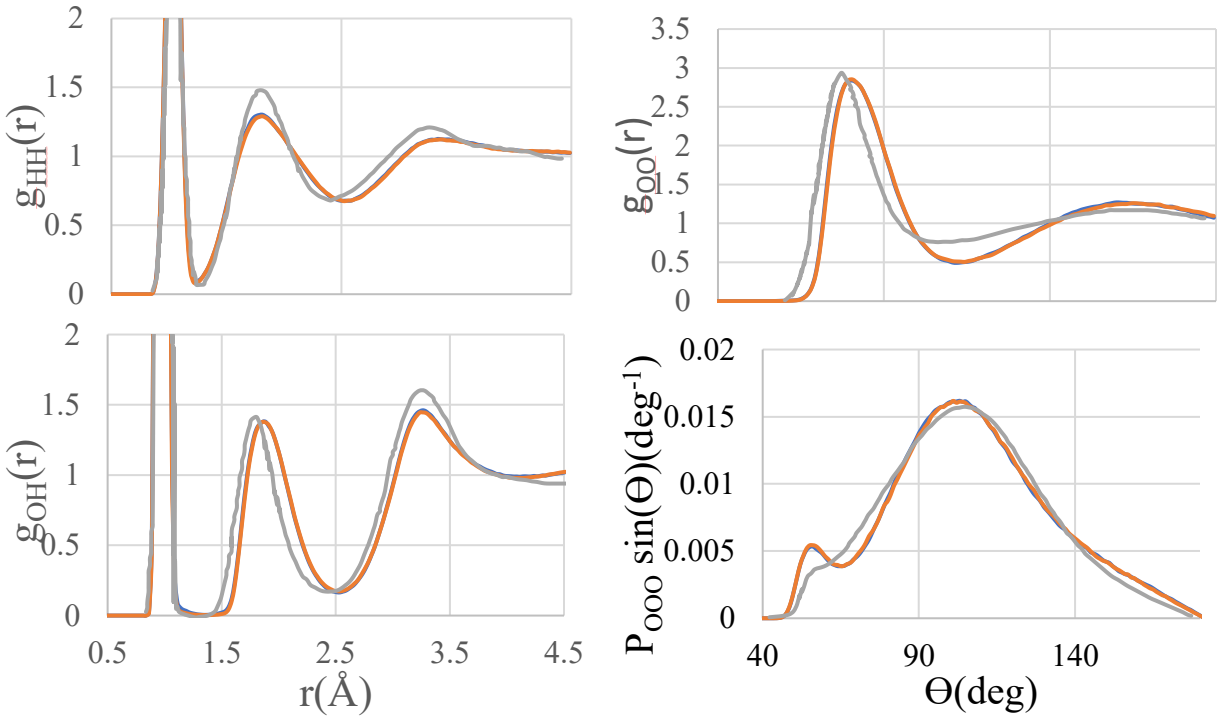

Figure 1: The g(r) for H-H (A) O-O (B) O-H (C) and the O-O-O bond angles (D)

Verification of the water precursor was done under NPT conditions at 300K. A cell of 1000 water molecules at 1.5 g/cm^3 density was generated with random positions using the PACKMOL [23] software. The system was then relaxed for 25 ps and the average volume and radial distributions of the O-H O-O and H-H bonds of the last 0.5 ps was taken. A single molecule of TMA was allowed to relax using ReaxFF geometry optimization, the bond lengths and angles were calculated and the same was done for DMA and MMA. Since neither of the models included three-body or four-body aluminum potentials, the ability to model a stable aluminum structure needs to be verified as well. A 20x20x20 crystal of 32,000 atoms is modeled from a primitive

cell of FCC Al acquired from the Materials Project database [24]. The crystal was then relaxed at temperatures within the functional ALD range (300K-600K) every 25K and was relaxed at each temperature for 2.5 ps. The relaxed volume at each temperature could then be used to calculate the lattice parameter (LP) and coefficient of thermal expansion (CTE) at those temperatures. The crystal was then heated from 300K to 1050K at a rate of **0**.08 K/fs under NPT conditions to determine the melting point of the crystal.

An Al(111) substrate 3 layers thick, 108 atoms, was generated using the USPEX substrate generator. An oxygen and DMA were introduced onto the surface and the geometries were optimized with a gradient convergence of **0.027 eV/Å and energy convergence of 2.7x10^{-4} eV**. A single H_2O molecule is then introduced into the system at a distance in which it would not interact with the surface, the geometry is then optimized again, and this pre-adsorption state is taken as the initial stage of the surface reaction. Three more images of the surface reaction (Adsorption of H_2O, Transition, and Desorption of CH_4) are optimized as well to get a full reaction path.

Results & Discussion

The structure of the water g(r)'s (Figure 1A-C) and the O-O-O angle distribution (Figure 1D) were in good agreement with published experimental [25] and computed [26]. The first g(OO) peak was shifted to the right by approximately 0.1Å from the reference and the second g(OH) peak was shifted 0.14Å to the right. Both models have identical peaks for all g(r)'s. The densities of the relaxed water systems were calculated to be 0.859 g/cm^3 for model 1 and 0.856 g/cm^3, 1.4 g/cm^3 lower than experimental result of 0.999 g/cm^3 [27]. This was likely due to the increase of the O-O and O-H bond lengths, indicating weaker bonds

Table 1: Bond lengths and angles of TMA, DMA, and MMA. Also included is the melting point and lattice parameter at 400K for Al crystal

TMA	Al-C	C-H	C-Al-C	H-C-H	Al-C-H
Model 1	1.9719	1.17	120	108.9	110
Model 2	1.9393	1.167	120	111.4	107.5
Berthomieu et al.	1.97	1.11	119.97	-	-
Almenningen et al.	1.964	1.113	-	-	111.8
DMA					
Model 1	1.96335	1.1725	115.9	109.2	109.8
Model 2	1.9294	1.1654	130.3	111.5	107.4
DFTB of DMACl	1.961	1.12	123.6	105	77.1
MMA					
Model 1	1.96167	1.174	-	109.2	109.7
Model 2	1.9169	1.1637	-	112	106.9
Al crystal	MP (K)	LP (@400K)			
Model 1	910	4.106			
Model 2	910	4.106			
Nakashia et al.	-	4.059			

described by the potentials. The bond distances of TMA (table 1) for Model 1 closely matched the references [28, 29] but the distances for model 2 were 0.04Å lower. This could be evidence of overcompensation of the Al-C bond potentials in model 2. This was evident in the Al-C sigma dissociation energy potential in the ReaxFF potential set. The sigma dissociation energy is 106.1950 for model 1 and 124.6651 for model 2. In the case of the C-H bond, neither model closely matched the references but did match each other. As expected, the C-H bond potentials are identical in the two models. The DMA results are compared against density functional tight binding (DFTB) of Dimethyl aluminum chloride. Model 1 was still the better fit of the Al-C bond length, and neither model 1 nor model 2 closely fit the C-H bond length. The overall length of the bonds decreased when losing methyl ligands in both the DMA and MMA cases. In both models the melting point of Al was calculated to be 910K, in good agreement with the known value of the melting point of aluminum. The lattice parameter 4.106Å at 400K. This lattice parameter is 0.05Å larger than the experimental value found in Nakashima et al. [30]

The adsorption of H_2O on DMA is a two-step process typical on the ALD process [3]. The reaction pathway for the adsorptions of first and second H_2O are shown in figure 2A and B. First a strong Al-O bond is formed spontaneously (-1.28 **eV** and -0.857 **eV** ΔE for model 1 and 2 respectively). Then an H transfers from the H_2O to one of the methyl ligands. The newly formed methane then desorbs from the center Al, leaving an OH and methyl ligand dangling surface. The reaction ends on an energy of -0.852 **eV** for model

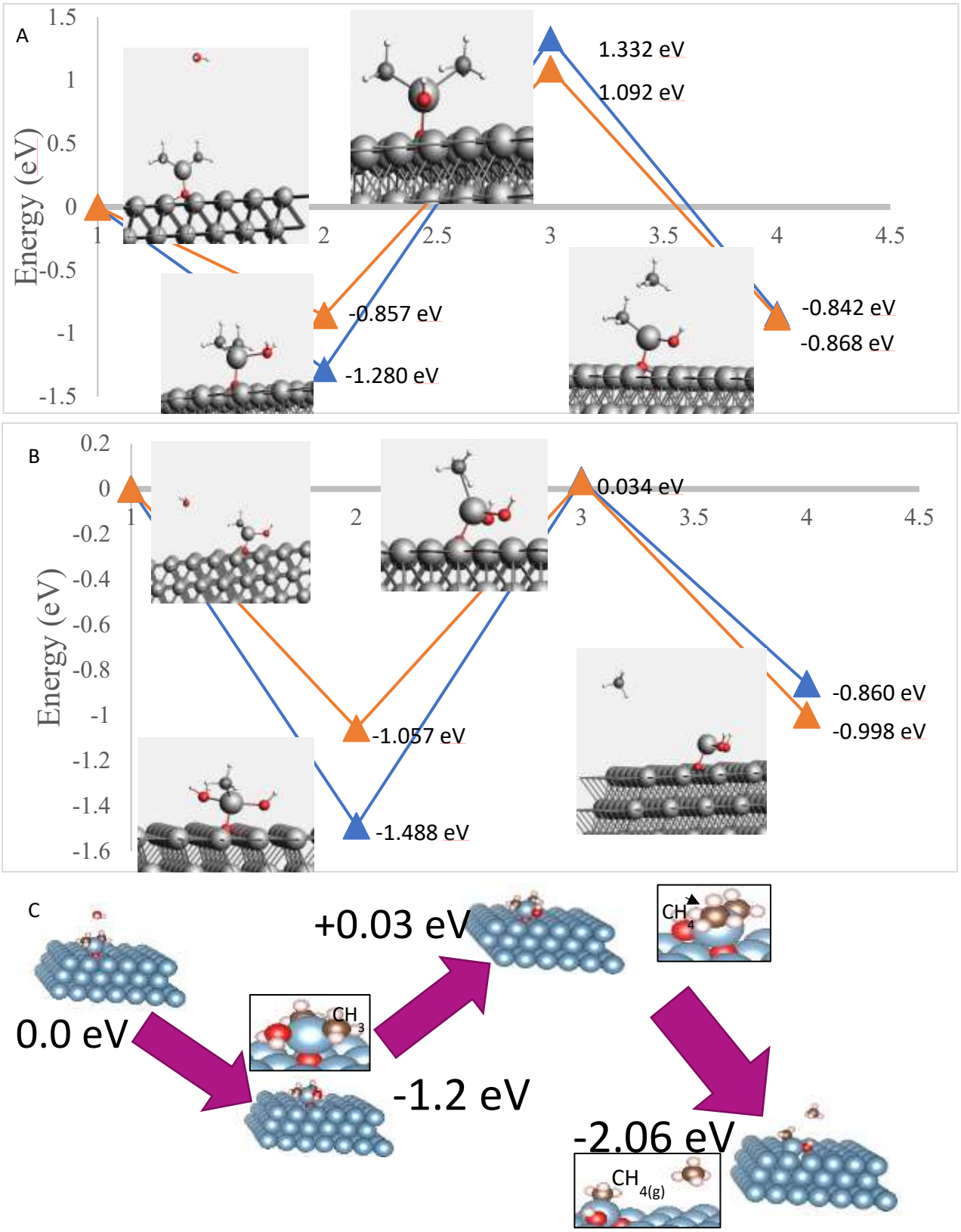

Figure 2: |-O-DMA +H_2O->|-O-DMA-H_2O->|O-MMA-OH +CH_4 (A) and |-$AlCH_3$-OH + H_2O -> |-$AlCH_3$-$(OH)_2$ + CH_4 (B) reaction pathways, and the VASP calculations of the |-O-DMA +H_2O->|-O-DMA-H_2O->|O-MMA-OH +CH_4 (C). Where | denotes the surface.

Table 2: Effective charges of DMA Al in three cases: H_2O adsorption to DMA bonded on O, bonded directly to Al substrate, and the second H_2O adsorption

	|-O-DMA + H_2O	|-O-DMA-H_2O	|-O-MMA-OH-CH_4	|-O-MMA-OH + CH_4
Model 1	0.8122	0.9923	1.0486	0.9054
Model 2	0.8022	0.9672	0.9834	0.8426
	|-DMA + H_2O	|-DMA-H_2O	|-MMA-OH-CH_4	|-MMA-OH + CH_4
Model 1	0.4797	0.7943	0.7591	0.5838
Model 2	0.4964	0.6874	0.8594	0.6101
	|-O-MMA-OH + H_2O	|-O-MMA-OH-H_2O	|-O-Al-$(OH)_2$-CH_4	|-O-Al-$(OH)_2$ +CH_4
Model 1	0.8983	1.0922	1.1541	0.9281
Model 2	0.8292	1.0077	0.9761	0.8045

1 and -0.868 **eV** for model 2. The hydrogen transfer represents a transition state with an energy barrier of 2.612 **eV** for model 1 and 1.949 **eV** for model 2. The adsorption of the second H_2O was also spontaneous with an energy barrier for the hydrogen transfer in the transition of 1.522 **eV** for model 1 and 1.091 **eV** for model 2 and the reaction is exothermic ending on an energy of -0.860 **eV** and -0.998 **eV** for model 1 and model 2 respectively. The large difference in energy for the two models during the desorption of the methyl ligand is explained by the difference in the potentials for the Al-C bond. The bond dissociation energy for model 2 is 124.6651. This shows that a higher loss of energy will occur when an Al-C bond is broken. which is evident in both reaction paths. Evidence of H-Al bonding between the hydrogen of the remaining OH and the central Al is evident in model 1, which would suggest a stronger bond between the two, confirmed by a higher bond energy in the potentials. The relative energy after the desorption of the methane is not lower than that of the H_2O adsorption in model 1 or 2 for the first or second adsorption/exchange events. This indicates that the ligand exchange and methane desorption are not favorable. This combined with the high energy barrier means that the ligand exchange will occur with the current force field potentials. The results published in Zheng et al. [19] show a spontaneous adsorption and a favorable ligand exchange event, a result that is shown in the VASP results for the formation of MMA.

To better understand the mechanism of adsorption of water onto DMA, the charges for the center Al for DMA bonded to an oxygenated surface, DMA bonded directly to the surface Al, and MMA bonded to an oxygenated surface were calculated [table 2]. We see that the charges for the DMA bonded on the oxygenated surface are higher than that of the Al bonded directly to the surface. This indicates the formation of a strong ionic bond for Al-O and a polarizing of the surface, making the system more favorable to the adsorption of H_2O.

Conclusions

A strategy to review the ALD of alumina utilizing Reactive Force Fields is in development. We have shown that stable precursors can be modeled using existing ReaxFF potentials. The aluminum substrate can be effectively modeled within the range of temperature for ReaxFF as well. Reaction paths for a single H_2O pulse of the ALD process have not been effectively modeled using potentials from two

different systems. Of the two models, model 1 described the precursor TMA better when reviewed against the literature. Model 2 showed surface chemistry that was energetically more favorable than model 1. Evidence that the training set used to develop the force field plays a large role in the transferability to additional systems. Further training of the potentials could lead to development of a potential that more accurately describes the surface chemistry for the ALD process. In the interest of developing these potentials, additional studies into the full interactions of both pulses needs to be conducted.

Acknowledgements

This project has received support from the National Science Foundation (NSF) (Grant No. 1809284) Electronics, Photonics and Magnetic Devices (EPMD) Program and it is gratefully acknowledged. We also thanks The National Energy Research Scientific Computing Center (NERSC) for computational support.

Data Availability

The datasets generated during and/or analyzed during the current study are available from the corresponding author on reasonable request.

Conflicts of Interests

On behalf of all authors, the corresponding author states that there is no conflict of interest.

References

1. George, S.M., *Atomic layer deposition: an overview.* Chem Rev, 2010. **110**(1): p. 111-31.
2. Puurunen, R.L., *Surface chemistry of atomic layer deposition: A case study for the trimethylaluminum/water process.* Journal of Applied Physics, 2005. **97**(12).
3. Widjaja, Y. and C.B. Musgrave, *Quantum chemical study of the mechanism of aluminum oxide atomic layer deposition.* Applied Physics Letters, 2002. **80**(18): p. 3304-3306.
4. Gakis, G.P., et al., *Investigation of the initial deposition steps and the interfacial layer of Atomic Layer Deposited (ALD) Al2O3 on Si.* Applied Surface Science, 2019. **492**: p. 245-254.
5. Goul, R., et al., *Electron tunneling properties of Al2O3 tunnel barrier made using atomic layer deposition in multilayer devices.* AIP Advances, 2019. **9**(2).
6. Salami, H., A. Poissant, and R.A. Adomaitis, *Anomalously high alumina atomic layer deposition growth per cycle during trimethylaluminum under-dosing conditions.* Journal of Vacuum Science & Technology A: Vacuum, Surfaces, and Films, 2017. **35**(1).
7. Strempel, V.E., et al., *Investigating the Trimethylaluminium/Water ALD Process on Mesoporous Silica by In Situ Gravimetric Monitoring.* Nanomaterials (Basel), 2018. **8**(6).
8. Xie, Y., et al., *Optimizing the process efficiency of atomic layer deposition of alumina for its sustainability improvement: a combined experimental and modeling study.* Journal of Cleaner Production, 2016. **133**: p. 338-347.
9. Elliot, A.J., et al. *Controlling the thickness of Josephson tunnel barriers with atomic layer deposition*. 2014. arXiv:1408.3077.
10. Shirazi, M. and S.D. Elliott, *Cooperation between adsorbates accounts for the activation of atomic layer deposition reactions.* Nanoscale, 2015. **7**(14): p. 6311-8.
11. Weckman, T. and K. Laasonen, *First principles study of the atomic layer deposition of alumina by TMA-H2O-process.* Phys Chem Chem Phys, 2015. **17**(26): p. 17322-34.

12. Groner, M.D., et al., *Low-Temperature Al2O3 Atomic Layer Deposition.* Chemistry of Materials, 2004. **16**(4): p. 639-645.
13. Cyster, M.J., et al., *Simulating the fabrication of aluminium oxide tunnel junctions.* npj Quantum Information, 2021. **7**(1).
14. Thompson, A.P., et al., *LAMMPS - a flexible simulation tool for particle-based materials modeling at the atomic, meso, and continuum scales.* Computer Physics Communications, 2022. **271**.
15. Stukowski, A., *Visualization and analysis of atomistic simulation data with OVITO–the Open Visualization Tool.* Modelling and Simulation in Materials Science and Engineering, 2010. **18**(1).
16. Chenoweth, K., A.C. van Duin, and W.A. Goddard, 3rd, *ReaxFF reactive force field for molecular dynamics simulations of hydrocarbon oxidation.* J Phys Chem A, 2008. **112**(5): p. 1040-53.
17. van Duin, A.C.T., et al., *ReaxFF: A Reactive Force Field for Hydrocarbons.* The Journal of Physical Chemistry A, 2001. **105**(41): p. 9396-9409.
18. Hong, S. and A.C.T. van Duin, *Atomistic-Scale Analysis of Carbon Coating and Its Effect on the Oxidation of Aluminum Nanoparticles by ReaxFF-Molecular Dynamics Simulations.* The Journal of Physical Chemistry C, 2016. **120**(17): p. 9464-9474.
19. Zheng, Y., et al., *Modeling and in Situ Probing of Surface Reactions in Atomic Layer Deposition.* ACS Appl Mater Interfaces, 2017. **9**(18): p. 15848-15856.
20. Kresse, G. and J. Furthmuller, *Efficient iterative schemes for ab initio total-energy calculations using a plane-wave basis set.* Phys Rev B Condens Matter, 1996. **54**(16): p. 11169-11186.
21. Perdew, J.P., K. Burke, and M. Ernzerhof, *Generalized Gradient Approximation Made Simple.* Phys Rev Lett, 1996. **77**(18): p. 3865-3868.
22. Kresse, G. and D. Joubert, *From ultrasoft pseudopotentials to the projector augmented-wave method.* Physical Review B, 1999. **59**(3): p. 1758-1775.
23. Martinez, L., et al., *PACKMOL: a package for building initial configurations for molecular dynamics simulations.* J Comput Chem, 2009. **30**(13): p. 2157-64.
24. Jain, A., et al., *Commentary: The Materials Project: A materials genome approach to accelerating materials innovation.* APL Materials, 2013. **1**(1).
25. de Kock, M.B., et al., *Determining the radial distribution function of water using electron scattering: A key to solution phase chemistry.* J Chem Phys, 2020. **153**(19): p. 194504.
26. LaCount, M.D. and F. Gygi, *Ensemble first-principles molecular dynamics simulations of water using the SCAN meta-GGA density functional.* J Chem Phys, 2019. **151**(16): p. 164101.
27. Sun, C.Q., *Scaling relation for the bond length, mass density, and packing order of water ice.* arXiv: Chemical Physics, 2013.
28. Almenningen, A., et al., *A Gas Phase Electron Diffraction Investigation of the Molecular Structures of Trimethylaluminium Monomer and Dimer.* Acta Chemica Scandinavica, 1971. **25**: p. 1937-1945.
29. Berthomieu, D., et al., *Trimethylaluminum Dimer Structure and Its Monomer Radical Cation: A Density Functional Study.* The Journal of Physical Chemistry A, 1998. **102**(40): p. 7821-7827.
30. Nakashima, P.N.H., *The Crystallography of Aluminum and Its Alloys*, in *Encyclopedia of Aluminum and Its Alloys*. 2019.